JOURNAL OF MATERIALS SCIENCE **38** (2003) 603–612

Elastic properties of wood with rectangular cross section under combined static axial force and torque

M. YAMASAKI
Laboratory of Biomechanics, Graduate School of Engineering Science, Osaka University, Toyonaka 560-8531, Japan
E-mail: mariko@me.es.osaka-u.ac.jp

Y. SASAKI
Laboratory of Biomaterial Engineering, Graduate School of Bioagricultural Sciences, Nagoya University, Nagoya 464-8601, Japan
E-mail: gasteig@agr.nagoya-u.ac.jp

It is rare for a component-member of a structure to be subjected to a simple stress state. Usually, it is subjected to a multi-axial stress state in many cases. Therefore, in order to more efficiently design a structure, it is necessary to fully understand the mechanical properties of constituent materials under such a state. In this report, the effect of combined axial force and torque loading on the elastic behavior of wood (Japanese beech and Japanese cypress) was examined. As the elastic behavior, the initial slopes of the stress-strain relationships obtained from combined loading tests are estimated. The specimen had a rectangular cross section with one of its major axes lying in the fiber (longitudinal) direction. The axial force and torque were applied in the fiber direction (along L) and about an axis lying in the L direction, respectively. Combined loading tests were performed using the proportional deformation loading method and the initial constant loading method. The results obtained were summarized as follows: (1) The effect of differences in loading methods on the relationships between shear stiffnesses and the states of combined stresses was confirmed, in particular, for Japanese cypress. (2) Differences in axial stiffness were observed between the two species under compression-shear combined stress state. While the axial stiffness of Japanese beech was not affected under the combined stress state, that of Japanese cypress tended to increase under compression-shear combined stress state. (3) The difference in shear or axial stiffness between the two planes was considered to be almost constant; however, when the axial or shear stress component of the combined stresses became dominant, the difference between the two planes tended to show a larger variation.

1. Introduction

Structural materials are rarely under uniaxial stress; rather, they are usually under biaxial or triaxial stress [1]. Therefore, in order to more efficiently design a structure, it is necessary to fully understand the behavior of materials under a state of combined stresses [1]. To date, studies of materials under biaxial or triaxial stresses have mainly focused on concrete and fiber reinforced composites [2–11]. The authors have conducted experiments on wood [12–14], which has not been the subject of as frequent investigations as other materials, and discussed its mechanical properties under combined axial force and torque. The major purpose of the previous studies that were based on combined loading tests was to examine failure properties. Parts of those studies have been previously presented by the authors [13, 14].

Stress-strain relationships are obtained from loading tests. The initial slopes of the relationships are used to evaluate the elastic moduli, which are important indices for characterizing the mechanical properties of materials in the elastic region [9]. As they are used extensively in the design of wood structures, it is important to understand how the stress-strain relationships or elastic properties behave under combined stresses which are, after all, the stress state acting on structures in real life [15].

In this study, we aim to investigate the effects of combined loading on the elastic behavior of wood. From the combined loading tests, two stress-strain relationships

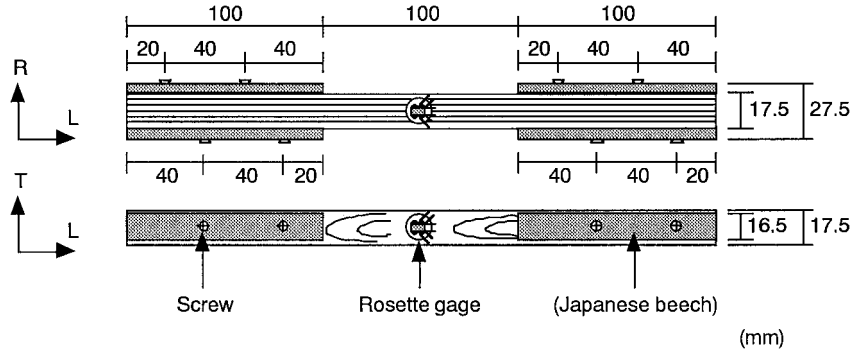

Figure 1 Rectangular test specimen (units: mm).

are obtained. The apparent stiffnesses under axial and shear stresses, which are estimated from the initial slopes of the stress-strain relationships obtained from combined static axial force and torque loading tests, are investigated to discuss the effects of combined stresses, differences in loading methods, and species of wood (Japanese beech and Japanese cypress).

2. Experiments

2.1. Specimen

Air-dried samples of two types of wood were tested, namely, Japanese beech (*Fagus crenata* B1.) and Japanese cypress (*Chamaecyparis obtusa* Endl.). Applying combined axial force and torque would produce a very complicated stress state on the surface of specimen if its grain axis was inclined to its loading axis. Therefore, in order to simplify the analysis, taking the anisotropy of the wood into consideration, the specimens were made to have a rectangular cross section with one of its major axes lying in the fiber direction, as shown in Fig. 1. The size of the specimens was 300 mm (L) × 17.5 mm (T) × 17.5 mm (R). The specimens were conditioned in a laboratory the temperature of which was maintained at 25°C and the relative humidity at 40%, until the weights of the specimens became constant. The specimens that were finally used in the tests were selected based on their specific gravity to minimize scatter in material quality. Table I shows the specific gravity, the moisture content, and the number of specimens used in the tests. As shown in Fig. 1, a grip was formed at the two ends of the specimen by attaching spliced pieces of Japanese beech on both sides using an epoxy resin adhesive and screws.

TABLE I Physical properties of specimens

Species	Number of specimens	Specific gravity	Moisture content (%)
Japanese beech	272	0.64 (0.05)	9.6 (0.2)
Japanese cypress	277	0.44 (0.01)	7.7 (0.3)

Numbers in parentheses mean standard deviation.

2.2. Test methods and loading methods

An electrohydraulic servo machine (EHF-ED 10/TD1-20L, manufactured by Shimadzu Corporation, Kyoto) for testing under combined axial force and torque was used. Axial force was applied in the fiber direction (along L) and torque was applied about an axis lying in the same direction as L. At each center of a cross grain plane (LT plane) and a straight grain plane (LR plane), a triaxial rosette gage (KFG-3-120-D17, manufactured by Kyowa Electronic Instruments Co., Ltd., Tokyo, with a gage length of 3 mm and 120 Ω) was attached. The applied axial force and torque, and the axial and rotational displacements were measured by load cells and electric displacement transducers on the testing machine itself, while the longitudinal and shear strains were measured by strain gages on the LT and LR planes. All tests were carried out in the laboratory of which temperature was maintained at 25°C and relative humidity at 40%.

2.2.1. Uniaxial loading test and pure torsion test

In order to determine the strengths in tension, compression and torque, uniaxial loading tests and pure torsion test were carried out under controlled conditions using a constant rate of displacement. Axial force was loaded at a constant axial displacement speed of 0.01 mm/s and torque was applied at a constant rotational speed of 0.05 deg/s. Assuming that failure occurs when stress is attained, the strength for each type of force was obtained based on the mean value of experimental failure stresses and is presented in Table II. These strengths then served as the basis upon which the initial constant loads for combined loading tests using the initial constant loading method were determined.

TABLE II Strengths of specimens

Species	Tension (MPa)	Compression (MPa)	Torque (N · m)	Shear (LT) (MPa)	Shear (LR) (MPa)
Japanese beech	63.8 (17.3)	51.9 (5.6)	25.2 (2.9)	21.4 (2.0)	23.7 (2.7)
Japanese cypress	63.9 (6.8)	38.1 (2.7)	20.7 (1.3)	18.3 (1.2)	19.3 (1.3)

Numbers in parentheses mean standard deviation. Ten specimens were tested for unitension, unicompression and pure torsion.

2.2.2. Proportional deformation loading

In the proportional deformation loading method, axial force and torque were applied simultaneously to the test specimen with the displacement speed of the applied axial force and the rotational speed of the applied torque kept constant. By changing the ratio of the application speeds of both displacements, a failure surface resulting from the combination of axial stress and shear stress at the time of failure was created. As loading was applied under controlled conditions using a constant rate of displacement, the displacement speed was set such that it did not exceed 1.5 times the speed used in uniaxial loading tests and pure torsion test so as to avoid the effect of impact forces.

2.2.3. Initial constant loading

In the initial constant loading method, axial force or torque was loaded over the initial constant loads (torque or axial force). Based on the strengths shown in Table II, the initial loads were set at five levels, equivalent to 20, 40, 60, 70 and 80% of each strength. Table III shows the values of the initial constant loads used in the tests. The loading was carried out under controlled conditions using a constant rate of displacement with the displacement speed of the axial force set at 0.01 mm/s and the rotation speed of the torque at 0.05 deg/s.

2.3. Evaluation method

2.3.1. Elastic property

The initial slope of the stress-strain relationship under the uniaxial stress state usually gives the elastic modulus. Two stress-strain relationships, one for axial and the other for shear, were obtained from the combined loading tests. These relationships were considered to show the influence of the two stresses on each other. In this study, their initial slopes were estimated as the apparent elastic modulus, that is, the apparent Young's modulus and the apparent shear modulus, which were interpreted as the axial and shear stiffnesses, respectively. The elastic properties under the combined stress state in this study were evaluated and discussed by using these axial and shear stiffnesses.

During the tests, data on axial force, torque and axial and shear strains on the LT and LR planes of the specimens were collected. Using these data, stress-strain relationships shown in Fig. 2 were obtained as examples. Here, axial stress σ_L was obtained by dividing the axial load by the cross-sectional area. The shear stresses at the center of the LT and LR planes, τ_{LT} and τ_{LR}, were obtained from Equation 1 [12, 16–21], when a rectangular-parallelepiped-shaped wood member was twisted around a major axis (in this case in the direction of the fiber length, L) as the central axis.

$$\left.\begin{aligned}\tau_{LT} &= \frac{T}{a^2 b\phi}\left[-2\left(\frac{2}{\pi}\right)^2\sqrt{\frac{G_{LT}}{G_{LR}}}\sum_{n=1}^{\infty}\frac{(-1)^{n-1}}{(2n-1)^2}\tanh\frac{(2n-1)\pi b}{2a}\sqrt{\frac{G_{LT}}{G_{LR}}}\right]\\ \tau_{LR} &= \frac{T}{a^2 b\phi}\left[1-2\left(\frac{2}{\pi}\right)^2\sum_{n=1}^{\infty}\frac{1}{(2n-1)^2}\left\{\cosh\frac{(2n-1)\pi b}{2a}\sqrt{\frac{G_{LT}}{G_{LR}}}\right\}^{-1}\right]\end{aligned}\right\} \quad (1)$$

where T is torque, a and b are the cross-sectional lengths of the specimen in the T and R directions, respectively, and G_{LT} and G_{LR} are shear moduli on the LT and LR planes, respectively. The quantity ϕ in the above equation can be expressed as shown in Equation 2:

$$\phi = \frac{1}{3} - \frac{2a}{b}\sqrt{\frac{G_{LR}}{G_{LT}}}\left(\frac{2}{\pi}\right)^5\sum_{n=1}^{\infty}\frac{1}{(2n-1)^5} \times \tanh\frac{(2n-1)\pi b}{2a}\sqrt{\frac{G_{LT}}{G_{LR}}} \quad (2)$$

TABLE III Values of initial constant loads

Species	Type of ramp load	Initial constant load: Type	Percentage of the maximum strength (%): 20	40	60	70	80	Units
Japanese beech	Torque	Tension	12.76	25.52	38.28	44.66	51.04	MPa
	Tension	Torque	5.04	10.09	15.13	17.65	20.17	N · m
	Torque	Compression	10.38	20.76	31.14	36.33	41.52	MPa
	Compression	Torque	5.04	10.09	15.13	17.65	20.17	N · m
Japanese cypress	Torque	Tension	12.78	25.56	38.34	44.73	51.12	MPa
	Tension	Torque	4.13	8.26	12.40	14.46	16.53	N · m
	Torque	Compression	7.62	15.24	22.86	26.67	30.48	MPa
	Compression	Torque	4.13	8.26	12.40	14.46	16.53	N · m

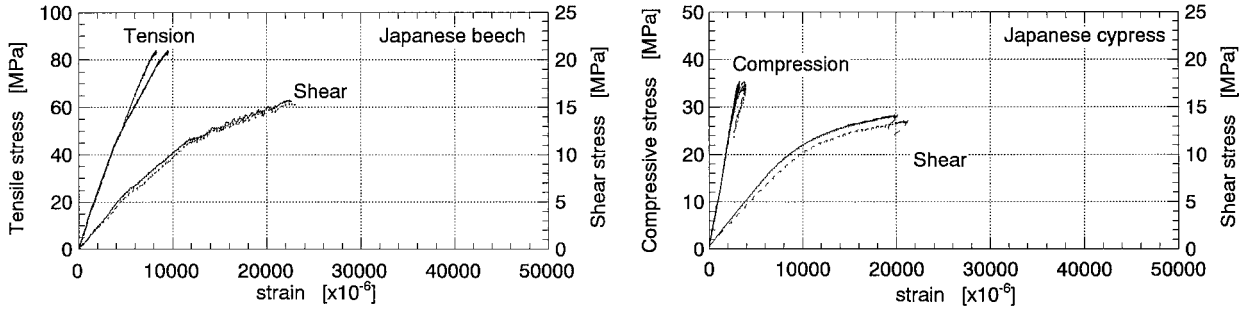

(a) Under tension-shear combined stress

(b) Under compression-shear combined stress

Figure 2 Relationship between stress and strain under axial-shear combined stresses, determined by the proportional deformation loading method. *Solid line*, LR plane; *dashed line*, LT plane.

Given that the initial slopes of the torque-shear strain curves directly measured on the LT and LR planes are k_{LT} and k_{LT}, respectively, Equation 3 can be deduced from Equation 1 as follows:

$$G_{LT} = \frac{k_{LT}}{a^2 b\phi}\left[-2\left(\frac{2}{\pi}\right)^2\sqrt{\frac{G_{LT}}{G_{LR}}}\sum_{n=1}^{\infty}\frac{(-1)^{n-1}}{(2n-1)^2}\tanh\frac{(2n-1)\pi b}{2a}\sqrt{\frac{G_{LT}}{G_{LR}}}\right]$$
$$G_{LR} = \frac{k_{LR}}{a^2 b\phi}\left[1-2\left(\frac{2}{\pi}\right)^2\sum_{n=1}^{\infty}\frac{1}{(2n-1)^2}\left\{\cosh\frac{(2n-1)\pi b}{2a}\sqrt{\frac{G_{LT}}{G_{LR}}}\right\}^{-1}\right] \quad (3)$$

The shear moduli, G_{LT} and G_{LR}, were computed as numerical calculation using Equation 3.

2.3.2. Combined stress state

In order to discuss the elastic behavior under combined loading, a combined stress state was proposed as follows [14]. Fig. 3 shows the relationships between shear stress and axial stress at the time of failure in which the dimensionless failure surface is obtained by dividing each stress by the mean value of its strength listed in Table II. The locus on this failure surface indicates both a failure condition and a combined stress state. Here, a given combined stress state on a dimensionless failure surface can be represented by the angle α from the shear stress axis, as depicted in the schematic diagram of Fig. 4. The angle α is given by Equation 4 as follows:

$$\alpha = \tan^{-1}\frac{\sigma_L/F_{aL}}{\tau/F_s} \quad (4)$$

where σ_L is the axial failure stress, τ is the shear failure stress on the LT or LR plane, F_{aL} is the axial strength and F_s is the shear strength on the LT or LR plane. When $\alpha = 0^\circ$, the state of stress is pure torsion, and as α increases, the state of stress becomes a combined stress state with the axial force becoming gradually dominant as α approaches $\pm 90^\circ$, and the state of stress becomes uniaxial when $\alpha = \pm 90^\circ$.

2.3.3. Statistical analysis

All data on the elastic properties were expressed as mean values (Mean) and standard deviations (S.D.) by classifying the combined stress states (angle α). They are shown in Tables IV and V. Statistical analyses were performed with the two-sample t-test following the test for equal variance (F-test). The two-sample t-test with

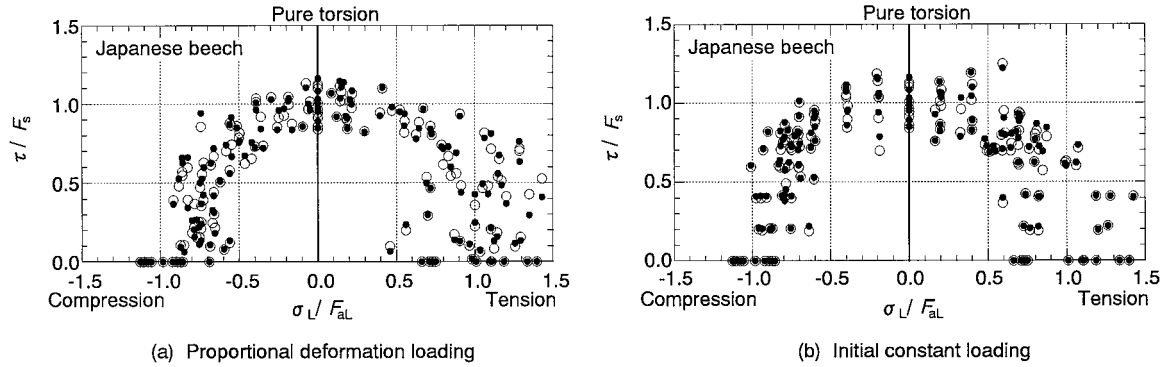

(a) Proportional deformation loading

(b) Initial constant loading

Figure 3 Dimensionless failure loci under axial-shear combined stresses. *Open circles*, LR plane; *filled circles*, LT plane; σ_L, axial failure stress; τ, shear failure stress on the LT or LR plane; F_{aL}, axial strength; F_s, shear strength on the LT or LR plane.

TABLE IV Apparent shear moduli under pure torsion and combined axial-shear stresses

State of stress	Loading method	Range of α (deg)	Plane	Japanese beech		Japanese cypress	
				Apparent shear modulus[a] (GPa)	P value[b]	Apparent shear modulus[a] (GPa)	P value[b]
Pure torsion	–	$\alpha = 0$	LT	0.94 (0.08)	–	1.09 (0.12)	–
			LR	1.30 (0.20)	–	1.23 (0.08)	–
Compression-shear combined stress	Proportional deformation loading	$-60\,(-50)^{c} < \alpha < 0$	LT	0.90 (0.19)	0.274	1.08 (0.15)	0.996
			LR	1.19 (0.17)	0.091	1.26 (0.11)	0.360
		$-90 < \alpha \leqq -60\,(-50)^{c}$	LT	0.91 (0.41)	0.714	1.40 (0.41)	0.0008**
			LR	1.29 (0.54)	0.956	1.52 (0.35)	0.0001**
	Initial constant loading	$-60\,(-50)^{c} < \alpha < 0$	LT	0.84 (0.14)	0.028*	0.99 (0.11)	0.012**
			LR	1.13 (0.16)	0.009**	1.14 (0.12)	0.011**
Tension-shear combined stress	Proportional deformation loading	$0 < \alpha < 60\,(50)^{c}$	LT	0.88 (0.16)	0.083	1.05 (0.10)	0.379
			LR	1.11 (0.11)	0.016*	1.25 (0.12)	0.579
		$60\,(50)^{c} \leqq \alpha < 90$	LT	0.86 (0.40)	0.379	0.82 (0.18)	0.00002**
			LR	1.27 (0.54)	0.797	1.06 (0.20)	0.00009**
	Initial constant loading	$0 < \alpha < 60\,(50)^{c}$	LT	0.90 (0.12)	0.320	0.99 (0.10)	0.016*
			LR	1.21 (0.12)	0.207	1.17 (0.10)	0.038*

[a]Numbers in parentheses mean standard deviation.
[b]Probability factors for significant difference between pure torsion and combined axial-shear stresses.
[c]Numbers in parentheses are for Japanese cypress and the other for Japanese beech.
*Indicate 95% significant.
**Indicate 99% significant.

TABLE V Apparent Young's moduli under uniaxial stresses and combined axial-shear stresses

State of stress	Loading method	Range of α (deg)	Plane	Japanese beech		Japanese cypress	
				Apparent Young's modulus[a] (GPa)	P value[b]	Apparent Young's modulus[a] (GPa)	P value[b]
Uniaxial compression	–	$\alpha = -90$	LT	10.85 (2.22)	–	10.12 (1.21)	–
			LR	10.97 (2.08)	–	10.53 (1.48)	–
Compression-shear combined stress	Proportional deformation loading	$-90 < \alpha < -30$	LT	10.50 (2.14)	0.646	11.90 (2.42)	0.002**
			LR	10.50 (2.31)	0.567	12.13 (2.38)	0.046*
		$-30 \leqq \alpha < 0$	LT	9.20 (3.03)	0.156	9.35 (2.34)	0.368
			LR	8.23 (2.63)	0.015*	11.30 (3.26)	0.456
	Initial constant loading	$-90 < \alpha < -30$	LT	9.54 (1.94)	0.084	11.32 (1.14)	0.007**
			LR	9.90 (1.69)	0.114	11.40 (1.33)	0.091
Uniaxial tension	–	$\alpha = 90$	LT	10.31 (1.86)	–	11.66 (1.38)	–
			LR	10.18 (1.52)	–	11.87 (1.71)	–
Tension-shear combined stress	Proportional deformation loading	$30 < \alpha < 90$	LT	9.76 (1.61)	0.371	11.45 (1.82)	0.693
			LR	10.26 (1.79)	0.888	11.81 (1.93)	0.924
		$0 < \alpha \leqq 30$	LT	8.52 (3.80)	0.206	9.31 (3.41)	0.014**
			LR	9.60 (2.38)	0.511	10.08 (3.11)	0.055
	Initial constant loading	$30 < \alpha < 90$	LT	9.88 (2.44)	0.627	10.82 (1.17)	0.048*
			LR	10.31 (2.53)	0.877	11.09 (1.36)	0.121

[a]Numbers in parentheses mean standard deviation.
[b]Probability factors for significant difference between uniaxial stresses and combined axial-shear stresses.
*Indicate 95% significant.
**Indicate 99% significant.

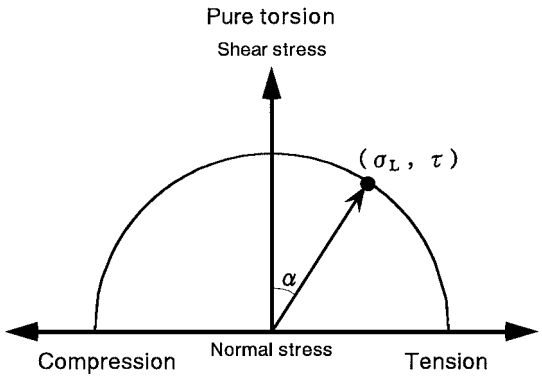

Figure 4 Schema of failure surface.

Welch's correction was adopted if two samples did not have equal variances. A value of $P < 0.05$ was taken as statistically significant.

3. Results and discussion

3.1. Effects of combined stress states and loading methods on elastic properties

3.1.1. Shear stiffness

Figs 5 and 6 show the relationships between apparent shear modulus as shear stiffness and angle α for Japanese beech and Japanese cypress, respectively. In both figures, (a) shows the results obtained by the proportional deformation loading method, and (b) shows

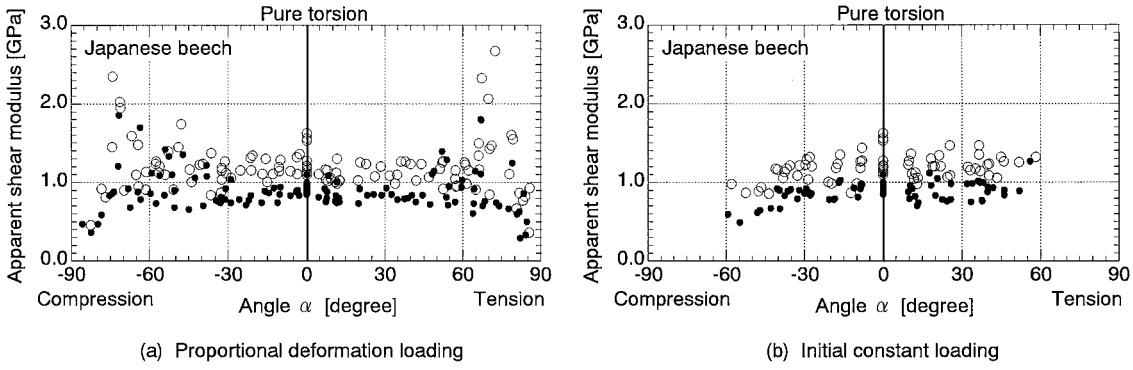

Figure 5 Relationship between the apparent shear modulus and the angle α for Japanese beech. *Open circles*, LR plane; *filled circles*, LT plane.

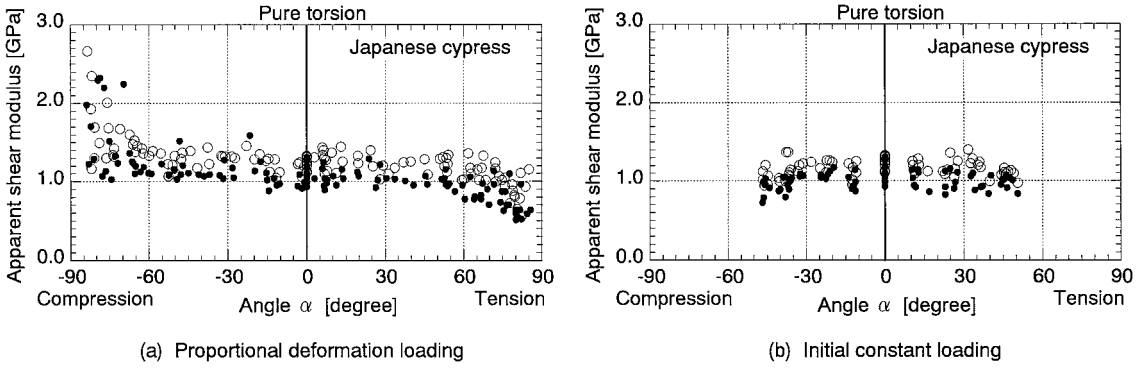

Figure 6 Relationship between the apparent shear modulus and the angle α for Japanese cypress. *Open circles*, LR plane; *filled circles*, LT plane.

the results obtained using the initial constant loading method. Table IV shows the shear stiffnesses and the comparisons with the shear moduli obtained from the pure torsion tests, by classifying the combined stress states by angle α. As shown in Figs 5b and 6b, the results of loading tests using the initial constant loading method existed in the range of $|\alpha| < 60^\circ$ for Japanese beech and $|\alpha| < 50^\circ$ for Japanese cypress, respectively. In order to further discuss the effect of the difference in loading method, the results for these ranges of $|\alpha|$ were also examined in Table IV.

From these figures and table, both species had similar tendencies over the range of $|\alpha| < 50^\circ$ or 60°, described as follows. In the case of proportional deformation loading, as shown in Figs 5a and 6a, the shear stiffness under both compression-shear and tension-shear combined stress states did not show a significant difference from that under pure torsion in most cases. Thus, it could be considered that there was no effect of the combined stress states on the shear stiffness, when the proportional deformation loading method was used.

On the other hand, as could be seen in Figs 5b and 6b, when the initial constant loading method was used, the shear stiffness showed a decrease compared to that from the pure torsion test. The effect of combined stresses was obvious in most cases, as shown in Table IV (for example, in the case of Japanese cypress under compression-shear combined stress, $P = 0.012$ (LT), 0.011(LR)). This might be due to the initial loading that caused some microscopic damage to the ultrastructure of the wood specimen, even if the axial force as the initial constant load had not reached the yield point [22]. Japanese cypress showed this tendency more clearly than Japanese beech. In addition, the shear stiffness of Japanese cypress obtained from the initial constant loading method was smaller than that from the proportional deformation loading method under both compression-shear and tension-shear combined stress states over the range of $|\alpha| < 50^\circ$ (99% significant in both cases). Therefore, the effect of the difference in loading method on the shear stiffness was obvious especially for Japanese cypress.

When the proportional deformation loading method was applied to Japanese cypress, as shown in Fig. 6a, the shear stiffness showed an increase under compression was applied dominant ($\alpha \leqq -50^\circ$) and a decrease when tension was applied dominantly ($\alpha \geqq 50^\circ$), compared to the shear modulus obtained from the pure torsion test (99% significant in both cases, as seen in Table IV). Therefore, the relationship between shear stiffness and angle α showed a clear tendency under the axial force was applied dominantly. When a large compression was applied with torsion, warping of the specimen by torsion was considered to be restrained. Under such a condition, the specimen is subjected to two kinds of torsional moments, one is torsional moment caused by twisting of the specimen, and the other is secondary torsional moment caused by the restraint of the warping. Torsional moment as the cross-sectional force is the sum of these torsional moments which caused by twisting of the specimen and the restraint of the warping [23–25]; as a result, the rotational angle is smaller than that under pure torsion [23–25]. This could be the reason why the shear stiffness became larger. In contrast, the case of the combined stress state where tension was dominant could be explained as follows: since the secondary torsional moment produced by the restraint of the warping might be negative under the state where

tension was dominant, the rotational angle was considered to be larger than that under pure torsion. Thus, the shear stiffness was considered to be smaller in contrast to the state where compression was dominant.

On the other hand, as can be seen in the case of Japanese beech in Fig. 5a, the behavior of the shear stiffness became increasingly unstable in the combined stress state in which the axial force was dominant ($|\alpha| \geqq 60°$), and no clear tendency could be discerned, unlike the case of Japanese cypress (Table IV). For Japanese beech, there were some cases in which bending of the specimen was observed when compression was dominant. The slenderness ratio of this specimen was about 20 considering the length of the central section of the specimen. Such a specimen might be bent when subjected to large compression [26, 27], especially when the material's quality was inhomogeneous [26, 27]. Because Japanese beech had more complicated tissue structure than Japanese cypress, it was more easily bent. This bending might cause both the center axes of the specimen and the load to slightly shift. Misalignment was considered to have some influence on the measurement of strains on both planes; therefore, the shear stiffness of Japanese beech was considered to be unstable.

Consequently, the shear stiffness of Japanese cypress exhibited a behavior distinct from that of Japanese beech for both loading methods. This suggests that Japanese cypress is likely to be more strongly affected by the state of combined stresses and loading method.

3.1.2. Axial stiffness

Figs 7 and 8 show the relationships between apparent Young's modulus as axial stiffness and angle α for Japanese beech and Japanese cypress, respectively. Table V shows the axial stiffnesses and the comparisons with Young's moduli obtained from uniaxial loading tests, by classifying the combined stress states by angle α. As shown in Figs 7b and 8b, the results of loading tests using the initial constant loading method existed in the range of $|\alpha| > 30°$ for both species. In order to further discuss the effect of the difference in loading method, the results for these ranges of $|\alpha|$ were examined in Table V.

As shown in Fig. 7b for Japanese beech, the axial stiffness under compression-shear combined stress state when using the initial constant loading method was slightly smaller than the Young's modulus that was obtained from the uniaxial compression test. However, this tendency was not significant, as seen in Table V. Moreover, when using the proportional deformation loading method, the axial stiffness was almost constant under both compression-shear and tension-shear combined stress states over the range of $|\alpha| > 30°$, as seen in Fig. 7a and Table V. Thus, it may be concluded that on the whole, the axial stiffness of Japanese beech is not affected by the combined stress states, as can be seen in Fig. 7.

On the other hand, as could be seen in Fig. 8a, when the proportional deformation loading method was applied to Japanese cypress, the axial stiffness under compression-shear combined stress state was larger than the Young's modulus obtained from the uniaxial compression test (99%(LT) and 95%(LR) significant as seen in Table V). Moreover, the axial stiffness under tension-shear combined stress state was not different from the Young's modulus obtained by the uniaxial tension test as seen in Table V, as was the case of Japanese

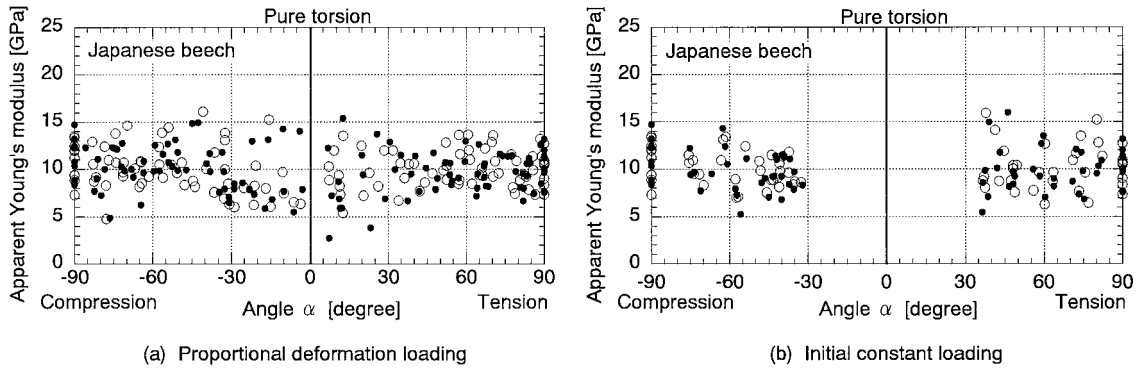

Figure 7 Relationship between the apparent Young's modulus and the angle α for Japanese beech. *Open circles*, LR plane; *filled circles*, LT plane.

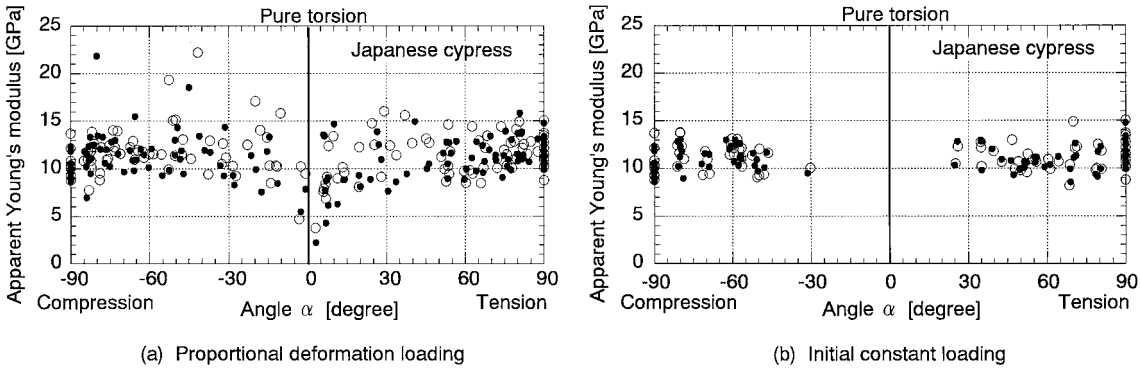

Figure 8 Relationship between the apparent Young's modulus and the angle α for Japanese cypress. *Open circles*, LR plane; *filled circles*, LT plane.

beech. In the case of initial constant loading, as shown in Fig. 8b, axial stiffness under compression-shear combined stress state was larger, as was the case of the proportional deformation loading method. However, under tension-shear combined stress state, Japanese cypress had smaller stiffness in the axial direction than the Young's modulus under uniaxial tension stress. This behavior was even more evident in the results on the LT plane, as shown in Table V. The tendency of the initial constant loading to decrease the axial stiffness under tension-shear combined stress state was similar to that of the shear stiffness as mentioned in the previous section.

As mentioned above, while the axial stiffness of Japanese beech was not affected by the combined stress states, that of Japanese cypress tended to increase under compression-shear combined stress state. Therefore, the behavior of the elastic property in the axial direction differed according to species especially under compression-shear combined stress state. Japanese cypress may be more resistant to compressive deformation when torsion is applied together with compression. Microscopic observation revealed that Japanese cypress is composed of mainly axial tracheids that comprise approximately 97% of the total volume [28–30]. They are long, narrow cells with lengths approximately 75–200 times (mostly 100 times) their diameters. Their lengths and diameters are, on average, 3.5 mm and 35 μm, respectively [28–30]. Japanese cypress tissue is structured like a bundle of long and narrow tubes. When torsion is applied on the bundle, it may take the form of a thrown string. Under compression-shear combined stress state, the bundle of axial tracheids in the form of a thrown string may strengthen themselves against the compressive deformation. In contrast, the major components of Japanese beech in the longitudinal direction, called vessel elements and fibers, are much shorter than axial tracheids of Japanese cypress, with an average length of approximately 1.0 mm [28–30]. Moreover, Japanese beech, being hardwood, is composed of various cell types, while Japanese cypress is softwood [28–30]. In the radial direction that intersects perpendicularly to the longitudinal direction, there are relatively hard cells called ray parenchyma, which comprise about 17.5% of the total volume [28–30]. Owing to such a tissue structure of Japanese beech, the axial elements may not take the form of a thrown string even if torsion is applied. Accordingly, it is considered that unlike Japanese cypress, Japanese beech does not have much resistance to compressive deformation.

3.2. Effect of combined stresses on the difference in stiffness between the two planes

Looking at the stiffnesses shown in Figs 5 to 8 measured on the LT and LR planes, the shear stiffness on the LR plane was seen to be larger than that on the LT plane (99% significant). Shear modulus on the LR plane is generally known to be larger than that on the LT plane, when pure torsion acts [26]. As for the axial stiffness, which should have the same value even if it was measured on the LT or LR plane, the mean value on the LR plane appeared to be larger than that on the LT plane, but the difference was not significant. These tendencies were observed in both species as well as for both loading methods.

Next, the change in the difference in stiffness between the two planes as a result of combined stresses is discussed by examining the ratios of stiffnesses on the LR plane to those on the LT plane. Figs 9 and 10 show the effect of combined stresses on each stiffness. The vertical axis in the figures shows the ratio as an index of the difference between the two planes. The value of 1.0 on the axis means that the stiffnesses on both planes have the same value. As shown in Figs 9b and 10b, the results of the initial constant loading method clearly indicated that both stiffnesses were not affected by the initial loading, indicating that the difference between the two planes was almost constant. Similarly, in the case of the proportional deformation loading method shown in Figs 9a and 10a, the difference was almost constant over the range of α in which the results of the initial constant loading method existed. Furthermore, the shear stiffness of Japanese beech showed a larger difference than that of Japanese cypress for both loading methods, as shown in Fig. 9, similar to that under pure torsion, which is generally known.

On the other hand, it is clear from Fig. 9a that the difference in shear stiffness between the two planes showed a larger scatter as axial stress became dominant in the combined stress state ($|\alpha| \geqq 60°$). Similarly, it is

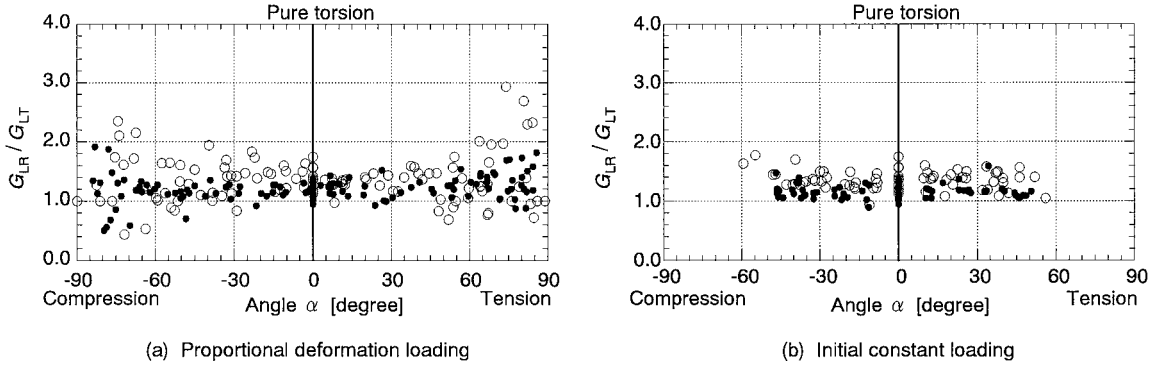

(a) Proportional deformation loading

(b) Initial constant loading

Figure 9 Effect of combined state of stress on the difference in the apparent shear modulus between the LT and LR planes. *Open circles*, Japanese beech; *filled circles*, Japanese cypress.

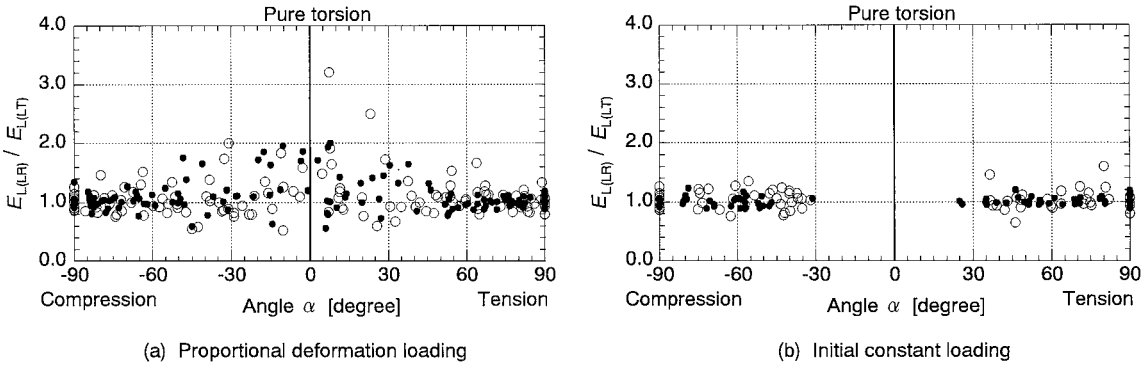

Figure 10 Effect of combined state of stress on the difference in the apparent Young's modulus between the LT and LR planes. *Open circles*, Japanese beech; *filled circles*, Japanese cypress; $E_{L(LT)}$, the apparent Young's modulus on the LT plane; $E_{L(LR)}$, the apparent Young's modulus on the LR plane.

clear from Fig. 10a that the difference in axial stiffness tended to have a larger scatter as shear stress became dominant (near $\alpha = 0°$). Thus, in the proportional deformation loading method, the shear stiffnesses on both planes showed a more pronounced difference as the axial stress component of the combined stresses became proportionally larger. Similarly, the axial stiffnesses on both planes showed a more pronounced difference as the shear stress component of the combined stresses became proportionally larger. The origins of these phenomena might be the shape of the specimen or the measuring method for strains in this study, under the state where one component of the combined stresses was dominant. For example, as mentioned in Section 3.3.1, bending that resulted from the slightly large slenderness ratio of this specimen was observed in Japanese beech to which compression was applied. Such problems might have led to the difference in stiffness between the two planes.

4. Conclusion

Focusing on axial-shear combined stresses, we discussed herein the effect of such combined stresses on the elastic properties of Japanese beech and Japanese cypress. The conclusions of this study are as follows:

(1) The effect of the difference in loading method on the relationship between the apparent shear moduli and the states of combined stresses was confirmed, in particular, for Japanese cypress.

(2) A difference in the axial stiffness under compression-shear combined stress state was observed between the two species. While the axial stiffness of Japanese beech was not affected by the combined stress state, that of Japanese cypress tended to increase under compression-shear combined stress state.

(3) The apparent elastic moduli of Japanese cypress seemed to be more sensitive to combined stresses than those of Japanese beech.

(4) The difference in stiffness between the two planes remained more or less unchanged over the range of α in which the results of both loading methods existed. On the other hand, in the proportional deformation loading method, the difference in either the shear or axial stiffness between the two planes tended to show a larger variation when either the axial stress or the shear stress component of the combined stresses became dominant, respectively.

For future studies, one issue that deserves special attention is the effect of tissue structure of wood on its mechanical properties under combined stresses. In discussing the effect of combined stresses on elastic properties, the approach using the angle α on the failure surface appears to be very effective. This approach makes it easier to consider the mechanical properties of materials under combined stresses from various viewpoints. Moreover, it enables comprehensive discussion of several properties, for example, failure strengths and elastic properties. Through such discussion, material behavior under combined stresses will be understood more clearly.

References

1. Y. TANIGAWA, H. OHTA, Y. OGATA, H. OHNO, R. KANEKO, K. KOIKE and K. YAMADA, in "Experimental Method for Structural Materials," 2nd ed. (Morikita Shuppan, Tokyo, 1991) p. 15 (in Japanese).
2. B. BRESLER and K. S. PISTER, *Trans. Am. Soc. Civil Eng.* **2897** (1955) 1049.
3. *Idem., J. Am. Concrete Institute* **55** (1958) 321.
4. T. OKAJIMA, *Trans. Architectural Inst. Jpn.* **182** (1971) 1.
5. S. C. COWIN, *Trans. of ASME, J. Appl. Mech.* **46** (1979) 832.
6. H. CEZAYIRLIOGLU, E. BAHNIUK, D. T. DAVY and K. G. HEIPLE, *J. Biomech.* **18** (1985) 61.
7. M. N. NAHAS, *J. Comp. Technol. Res.* **8** (1986) 138.
8. M. J. OWEN and J. R. GRIFFITHS, *J. Mater. Sci.* **13** (1978) 1521.
9. S. AMIJIMA, T. FUJII, T. SAGAMI and T. MATSUOKA, *J. Soc. Mat. Sci. Jpn.* **38** (1989) 347.
10. S. AMIJIMA, T. FUJII and M. HAMAGUCHI, *Composites* **22** (1991) 281.
11. T. FUJII, S. AMIJIMA and F. LIN, *J. Composite Mat.* **26** (1992) 2493.
12. K. ORIGUCHI, H. YOSHIHARA and M. OHTA, *J. Soc. Mat. Sci. Jpn.* **46** (1997) 385.
13. M. YAMASAKI, Y. SASAKI and K. ANDO, *J. Jpn. Wood. Res. Soc.* **45** (1999) 297.
14. M. YAMASAKI and Y. SASAKI, *Trans. Jpn. Soc. Mech. Eng.* **66** (2000) 1612.
15. The Japan Society of Mechanical Engineers, in "The Modulus of Elasticity of Metals and Alloys" (Jpn. Soc. Mech. Eng., Tokyo, 1980) p. 10 (in Japanese).
16. A. E. H. LOVE, in "A Treatise on the Mathematical Theory of Elasticity" (Dover, New York, 1927) p. 310.
17. R. F. S. HEARMON, in "Elastic of Wood and Plywood" (Her Majesty's Stationery Office, London, 1948) p. 10.

18. *Idem.*, in "An Introduction to Applied Anisotropic Elasticity" (Oxford University Press, London, 1961) p. 51.
19. K. OKUSA, *J. Jpn. Wood. Res. Soc.* **23** (1977) 217.
20. N. SUZUKI and Y. OKOHIRA, *Bull. Fac. Agr. Mie. Univ.* **65** (1982) 41.
21. H. YOSHIHARA and M. OHTA, *J. Jpn. Wood. Res. Soc.* **39** (1996) 993.
22. R. KITAHARA, J. TSUTSUMI and T. MATSUMOTO, *ibid.* **27** (1981) 1.
23. H. WAGNER and W. PRETSCHNER, *Luftfahrtforschun* **11** (1935) 174.
24. S. KOMATSU, in "Theory and Calculation for Thin-Walled Structures. I" (Sankaido, Tokyo, 1969) p. 218 (in Japanese).
25. N. TAKAOKA, in "Torsion Analysis of Structural Members" (Kyoritsu Shuppan, Tokyo, 1974) p. 77 (in Japanese).
26. H. WATANABE, in "Review of Wood Science" (Nohrin Shuppan, Tokyo, 1978) p. 460 (in Japanese).
27. L. VORREITER, in "Holztechnologisches Handbuch," Bd. I. (Verlag Georg Fromme & Co., Wien, 1949) p. 226 (in German).
28. J. G. HAYGREEN and J. L. BOWYER, in "Forest Products and Wood Science, an Introduction," 2nd ed. (Iowa State University Press/AMES, Iowa, 1989) p. 57.
29. G. TSOUMIS, in "Science and Technology of Wood" (Van Norstrand Reinhold, New York, 1991) p. 14.
30. K. SHIMAJI, S. SUDO and H. HARADA, in "Anatomical Structure of Wood" (Morikita Shuppan, Tokyo, 1976) p. 111 (in Japanese).

Received 10 July 2001
and accepted 16 October 2002